Bioresource Technology 449 (2026) 134365

Contents lists available at ScienceDirect

Bioresource Technology

journal homepage: www.elsevier.com/locate/biortech

# Modeling thermophilic syntrophic VFA oxidation using thermodynamic principles: Insights from enrichment cultures

Sahak Yeghiazaryan [a], Gabriel Capson-Tojo [a], Jean-Philippe Steyer [a], Maria Westerholm [b], Nicolas Bernet [a], Simon Labarthe [c,d], Elie Desmond-Le Quemener [a,*]

[a] INRAE, Univ. Montpellier, LBE, 102 Avenue des étangs, F-11100 Narbonne, France
[b] Department of Molecular Sciences, Swedish University of Agricultural Sciences, Uppsala SE-750 07, Sweden
[c] University of Bordeaux, INRAE, BIOGECO, F-33610 Cestas, France
[d] University of Bordeaux, INRAE, F-33400 Talence, France

## HIGHLIGHTS

- Validated parameters for syntrophs in thermophilic, high-ammonia conditions.
- Thermodynamic constraints ($M_{Th}$ model) reduce parameters, improve identifiability.
- $M_{Th}$ predicts realistic growth yields, consistent with literature and qPCR data.
- $M_{Th}$ highlights energy limits and identifies gaps in syntrophs metabolism.

## GRAPHICAL ABSTRACT

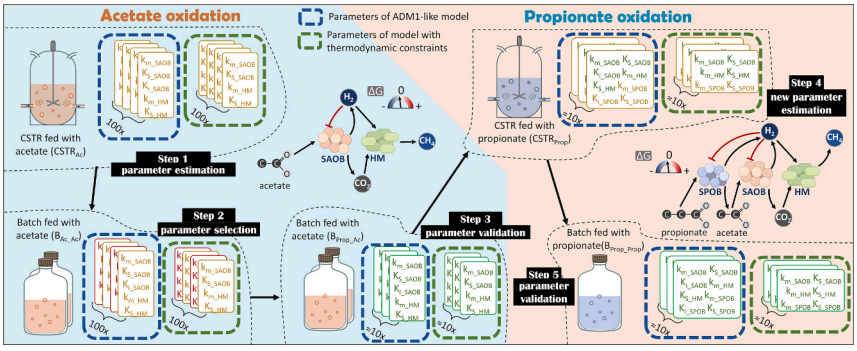


## ARTICLE INFO

*Keywords:*
Syntrophy
Biogas
Thermophilic anaerobic digestion
Modeling
Thermodynamics

## ABSTRACT

In anaerobic digestion, high ammonia concentration and thermophilic conditions inhibit acetoclastic methanogens, favoring syntrophic oxidation of volatile fatty acids. In the well-known ADM1 model, however, syntrophic oxidation of acetate is not included. In this study, we estimated and validated kinetic parameters of syntrophic acetate oxidizing bacteria (SAOB) and associated syntrophs (syntrophic propionate oxidizing bacteria (SPOB), hydrogenotrophic methanogen (HM)) using data from dedicated enrichment experiments. Syntrophic interactions are inherently constrained by thermodynamics, requiring tight cooperation between partners to make methanogenesis possible. We thus compared a classical ADM1-based approach ($M_{AMD1}$) with a thermodynamically constrained version ($M_{Th}$) that includes estimation of growth yields and inhibition directly from thermodynamic principles. Both modeling approaches enabled successful parameter estimation, but $M_{Th}$ had several advantages: by reducing the number of empirical parameters and enforcing thermodynamic feasibility, it improved parameter identifiability and provided more realistic growth yields, although uncertainties in half-saturation constants ($K_S$) remain relatively high. The analysis further revealed that, unlike SPOB and HM, SAOB cannot generate ATP through substrate oxidation alone yet still exhibit growth. This paradox points to missing or poorly understood metabolic pathways (e.g., alternative electron shuttle or energy conservation

* Corresponding author.
*E-mail addresses:* sahak.yeghiazaryan@inrae.fr (S. Yeghiazaryan), Elie.Le-Quemener@inrae.fr (E. Desmond-Le Quemener).

https://doi.org/10.1016/j.biortech.2026.134365
Received 28 November 2025; Received in revised form 20 February 2026; Accepted 5 March 2026
Available online 7 March 2026

mechanisms). Overall, the study provides validated parameter ranges for syntrophic partners under thermophilic and high-ammonia conditions and demonstrates the added value of incorporating thermodynamic constraints in ADM1-type models to improve robustness and reveal knowledge gaps in microbial energy metabolism.

## 1. Introduction

Biogas from biomass bioprocessing is a sustainable alternative to fossil fuels (Pantaleo et al., 2013; Viancelli et al., 2019). In anaerobic digestion (AD), organic substrates are converted by anaerobic microorganisms into digestate and methane-rich biogas, which serve as ertilizer and a versatile renewable energy carrier respectively (2019).

The microbial conversion in AD proceeds through four phases: hydrolysis, acidogenesis, acetogenesis, and methanogenesis (Meegoda et al., 2018; Wang et al., 2009). During hydrolysis, complex organic materials, including proteins, fats, and carbohydrates, are converted into simpler molecules such as amino acids, fatty acids, or oligopeptides (Heukelekian, 1958). In acidogenesis, these compounds are further converted into volatile fatty acids (VFA) such as propionate and butyrate, or alcohols (Gujer and Zehnder, 1983). Acetogenesis then oxidizes these intermediates to acetate and $H_2$ or formate. In the final methanogenesis step, acetate, formate, and $H_2$ are converted into methane (McCarty and Smith, 2002; McInerney and Bryant, 1981).

Methane is produced either via acetoclastic methanogenesis, where acetate is directly cleaved or via hydrogenotrophic methanogenesis, where $CO_2$ is reduced using $H_2$ or formate (Boone et al., 1989; Hattori et al., 2001; Pan et al., 2016). In protein-rich substrates (such as food waste), protein hydrolysis can generate high ammonia levels, which inhibit sensitive microorganisms, particularly acetoclastic methanogens (Capson-Tojo et al., 2020; Chen et al., 2014; Rajagopal et al., 2013; Westerholm et al., 2011). Depletion or decrease in activity of acetoclastic methanogens induces acetate accumulation, risking reactor acidification and process failure. Under these conditions, acetate can be oxidized to $CO_2$ by syntrophic acetate-oxidizing bacteria (SAOB) (Schnürer and Nordberg, 2008; Westerholm et al., 2011). The released electrons, transferred as $H_2$, formate, or through direct interspecies electron transfer (DIET), are then used by hydrogenotrophic methanogens (HM) to reduce $CO_2$ to methane (Hattori et al., 2001; Schink, 1997; Westerholm et al., 2019, 2011). Such a shift from acetoclastic to hydrogenotrophic methanogenesis is also observed during the transition from mesophilic to thermophilic temperature conditions (Wett et al., 2014), which may reflect both the intrinsic temperature sensitivity of acetoclastic methanogens and the shift in the $NH_3/NH_4^+$ equilibrium at higher temperatures, leading to increased free $NH_3$ and therefore stronger inhibition. The oxidation of VFAs is thermodynamically unfavorable under standard conditions and only proceeds when $H_2$ or formate concentrations are kept sufficiently low (Dolfing, 2014; Scholten and Conrad, 2000; Westerholm et al., 2019). This requires a tight coupling between hydrogen-producing and hydrogen-consuming microorganisms, an obligate cooperation that defines syntrophy and underscores the key role of thermodynamics in governing both the feasibility and kinetics of these processes. However, even when syntrophic acetate oxidation (SAO) establishes, the low energy yield of SAO constrains SAOB growth rates. As a result, acetate may accumulate, leading to reduced methane production and, in extreme cases, acidification and inhibition of methanogenesis. A proper characterization of SAOB and of the thermodynamic and kinetic constraints governing SAO is thus crucial to model, operate and control anaerobic digesters under such conditions.

Modeling biological processes can help make predictions and assumptions that can guide strategies to optimize processes and efficient experimental design. Among available models for anaerobic digestion, the anaerobic digestion model ADM1 is well known and widely applied. Although originally developed for modeling sludge digestion in wastewater treatment plants (WWTP) (Batstone et al., 2002), it can be adapted, with some modifications, to describe the digestion of other substrates (Antonopoulou et al., 2012; Mo et al., 2023). This can be achieved by recalibration of certain parameters or modifying the model structure (*e.g.*, addition of processes and state variables). In its default version, ADM1 assumes the conversion of acetate into methane through acetoclastic methanogenesis only. When adapting ADM1 to model food waste digestion, sensitivity analysis revealed acetate uptake parameters to be among most influential parameters (Zhao et al., 2019). Even more the inclusion of syntrophic acetate oxidation in the ADM1 model has been showed to improve predictions of food waste digestion in mesophilic (Capson-Tojo et al., 2021; Yang et al., 2020) or thermophilic (Montecchio et al., 2017; Rivera-Salvador et al., 2014; Wett et al., 2014) conditions. Those results reveal that inclusion of syntrophic acetate oxidation can improve ADM1 model predictions of non-diluted waste. But in before mentioned works, parameters of SAOB have not been identified on data from dedicated experiments of SAOB and associated syntrophs in high ammonia conditions, to have more robust predictions.

Since syntrophic oxidation of VFAs to methane occurs close to thermodynamic equilibrium, the incorporation of thermodynamics can be important when modeling this process. In the ADM1 model, the classical Monod equation is used to describe the kinetics of substrate consumption. However, this equation is insufficient for reactions operating near thermodynamic equilibrium (Hoh and Cord-Ruwisch, 1996; Jin and Bethke, 2003). Thermodynamics can be incorporated by calculating Gibbs free energy and using it to estimate growth yield and potential inhibition (Kleerebezem and Van Loosdrecht, 2010). The incorporation of thermodynamics into ADM1 has been proposed for modelling syntrophic propionate oxidizers (SPOB) (Patón and Rodríguez, 2019a) to prevent thermodynamically unfavorable conversions and later refined through a recalibration of the parameters corresponding to SPOB and HM (Singh et al., 2023). However, to our knowledge, thermodynamics in a model have not yet been integrated into models of communities, in which acetate is converted by SAOB and HM.

In this study, SAOB and its associated syntrophs (SPOB and HM) were modeled. Parameter estimation and validation were based on data from thermophilic enrichment reactors previously operated with either propionate or acetate. Using enrichment cultures allowed us to focus on a well-characterized community and to reduce the complexity inherent to anaerobic digestion, thereby enabling more reliable parameter estimation. To identify the most suitable modeling approach, several ADM1-like model variants were evaluated, including the classical ADM1 formulation and thermodynamics-based versions. Their performance was compared in terms of prediction accuracy, parameter distribution, and uncertainty.

## 2. Materials and methods

### 2.1. Experimental data used for calibration and validation

Experimental data from (Singh et al., 2023) were used (Fig. 1). The inoculum originated from an industrial-scale biogas reactor treating food waste (Westerholm et al., 2020). Microbial communities were cultivated in continuous stirred-tank reactors (CSTRs) fed with either propionate or acetate ($CSTR_{Prop}$, $CSTR_{Ac}$) as the sole energy and carbon source. The reactors operated under thermophilic conditions (52 °C) and received an anaerobic medium containing propionate and acetate (≈ 0.3 M) and high ammonia levels (8.9 g $L^{-1}$ ammonium chloride), and yeast extract. In the CSTR experiments, the dilution rate was 26 μL/min, with an influent medium containing 0.1 M of substrate (propionate in

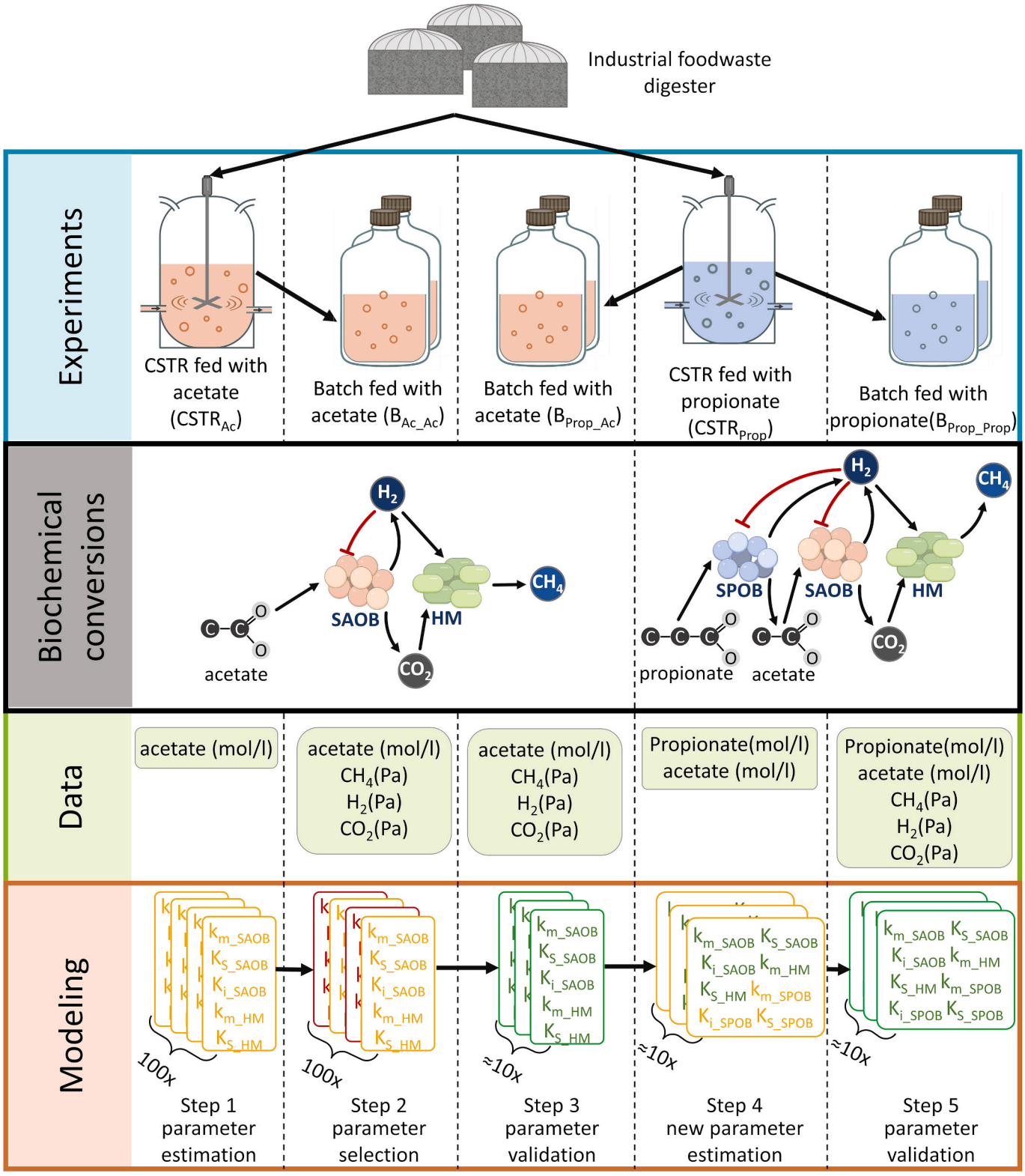


**Fig. 1.** Schema of the experiments carried out, biochemical conversions, data available from experiments and parameter optimization and validation procedure. Top row indicates the 2 CSTR and 3 batch experiments that were conducted, with dedicated substrates (Singh et al., 2023). In the second row, the different bioprocesses at play are presented for acetate (left) and propionate (right) fed experiments. In the third row, the metabolite that were screened are indicated for each experiment. In the last row, the five-step estimation procedure is indicated. Step 1: SAOB and HM parameters were fitted with a Monte-Carlo procedure. Step 2: Best parameter sets were selected on $B_{Ac\_Ac}$ data. Step 3: optimal parameters were validated on an external data set ($B_{Prop\_Ac}$). Step 4: SPOB parameters were fitted. Step 5: the data are validated on an external data set ($B_{Prop\_Prop}$). For model parameters yellow color shows that parameters are estimated, red color that parameters are rejected and green that parameters are validated.

$CSTR_{Prop}$ and acetate in $CSTR_{Ac}$) and 0.95 M of carbonate added as carbonate buffer (Singh et al., 2023). Because a single specific carbon source was added to the reactors, this led to the selection of simplified desired microbial communities from the more complex initial community in both reactors after 630 days of operation. The enriched propionate-degrading culture developed in $CSTR_{Prop}$ was relatively more metabolically complex than in $CSTR_{Ac}$ since SPOB were also enriched alongside SAOB and HM. After the CSTR operation, duplicate batch reactors were inoculated with 0.5 L of inoculum culture from the reactors. Two duplicates were inoculated with culture from $CSTR_{Prop}$, where one set was fed with acetate ($B_{Prop\_Ac}$) and one with propionate ($B_{Prop\_Prop}$). Another set-up of duplicate batches was inoculated with enrichment culture from $CSTR_{Ac}$ and fed with acetate ($B_{Ac\_Ac}$). Inoculation was done by converting the CSTR into a fed-batch reactor, closing the outflow to increase the total volume of the medium. After transfer, the batches were allowed to acclimatize for a few days, before propionate or acetate was added. At day 32, from reactors $B_{Prop\_Prop}$ and $B_{Prop\_Ac}$, headspace gas was released since the internal pressure had risen to approximately 2 bar. The partial pressure of gases was measured before and after the release of gases.

In the CSTRs, different VFAs concentrations were measured, but only propionate and/or acetate were detected. Additionally, pH and volume of liquid were also measured. In the batch experiments, VFA, $H_2$, $CH_4$, and $CO_2$ and partial pressures in the headspace were determined. In some batch experiments ($B_{Prop\_Ac}$, $B_{Prop\_Prop}$), the initial acetate concentration and $H_2$ partial pressure were not measured (Singh et al., 2023). These missing values were estimated through data imputation by using the interpolate.make_smoothing_spline() function from Scipy package (Virtanen et al., 2020) to perform interpolation and obtain estimates of the initial values, essential for modelling purpose. To estimate the sensitivity of model predictions of estimated values, the accuracy change of the model prediction were measured in $B_{Prop\_Prop}$ reactor data by varying estimated values in the range of ± 20% (see Table S6 in Supplementary Material). Analysis showed that the variation of estimated values had small effect on the accuracy of predictions.

### 2.2. Description of the models

In this work, two main models were compared (Table 1). These models encompass three microorganism clades (SAOB, methanogens, and SPOB), include an inhibition term (eq. (1) and biomass decay. Kinetics of substrates consumption were implemented using a Monod-type equation:

$$\frac{\partial S}{\partial t} = \nu_S \bullet \frac{k_m \bullet S}{K_s + S} \bullet X \bullet I \quad (1)$$

where $S$ is the substrate concentration at a time point, $I$ is the inhibition term, $X$ is the biomass concentration, $k_m$ is the maximum uptake rate, $K_s$ is the half saturation constant, and $\nu_s$ is the stoichiometric coefficient (see how defined in the matrix in Supplementary material). The inhibition term allows to model the inhibition of microorganisms by $H_2$ accumulation (see section "Inhibition function"). The time integration of equation (1) is implemented by providing its right-hand side to a LSODA time integrator in the scientific computing Python package SciPy (see section 2.6 Model implementation for further details).

Reactions of catabolism (eq. 2, 4, 6) and anabolism (eq. 3, 5, 7) of syntrophic propionate and acetate conversion to methane are taken into account in the model. A generalized formula of biomass $CH_{1.8}O_{0.5}N_{0.2}$ to make anabolism reactions was used according to (Kleerebezem and Van Loosdrecht, 2010).

$CH_3\text{-}CH_2\text{-}COO^- + 2H_2O \rightarrow CH_3\text{-}COO^- + 3H_2 + CO_2$ (2).

$0.3CH_3\text{-}CH_2\text{-}COO^- + 0.2NH_4^+ + 0.2CO_2 \rightarrow CH_{1.8}O_{0.5}N_{0.2} + 0.1HCO_3^- + 0{\cdot}.2H_2O$ (3).

$CH_3\text{-}COO^- + H^+ + 2H_2O \rightarrow 2CO_2 + 4H_2$ (4).

$0.525CH_3\text{-}COO^- + 0.2NH_4+ + 0.275CO_2 \rightarrow CH_{1.8}O_{0.5}N_{0.2} + 0.325HCO_3^- + 0{\cdot}.125H_2O$ (5).

$4H_2 + CO_2 \rightarrow CH_4 + 2H_2O$ (6).

$2.1H_2 + 0.2NH_4^+ + 0.8CO_2 + 0.2HCO_3^- \rightarrow CH_{1.8}O_{0.5}N_{0.2} + 1{\cdot}.7H_2O$ (7).

The decay rate constant was set to the default value from the ADM1 model. Gas-liquid mass transfer was included using a similar implementation as in ADM1 (21): gas solubility was estimated using Henry's law, and the gas–liquid transfer coefficient ($k_La$) was set to the default value from ADM1. The $k_La$ value of ADM1 is high, but since experiments have been conducted over long periods and substrate uptake rates were relatively slow, it was decided to use it anyway as gas–liquid transfer is not limiting in these conditions. Additionally, the model accounted for the chemical equilibrium between $CO_2$ and $HCO_3^-$. For the CSTR experiments, gas outflow was implemented as in the ADM1 model. The headspace was assumed to be initially filled with $N_2$ gas.

First, a model based on a simplified version of the ADM1 ($M_{ADM1}$) was obtained by modeling inhibition and growth yields in a similar way to ADM1 (see Table 1). The explicit expression of inhibition is indicated in the section « Inhibition function ».

Then, models describing the same community, including thermodynamics, were built up ($M_{Th}$) (see section "Thermodynamics calculations"). In this version of the model, inhibition and growth yield were calculated from thermodynamic principles (see section « Thermodynamics calculations »). Compared to the ADM1-like model, it requires fewer parameters to estimate, as there are no inhibition parameters (see section « Parameter estimation and validation »). Inclusion of thermodynamics also prevents the model from predicting reactions under unfavorable and therefore unrealistic conditions.

In order to better explore $M_{ADM1}$ and $M_{Th}$ models, model modifications were tested (Table 1). In the $M_{ADM1}$ simulations, inhibition term was very low and constant most of the time (indicating a strong inhibition). In $M_{Th}$ simulations, inhibition term was also constant most of the time but had a value close to 1 (meaning no or little inhibition). Because of this behavior of inhibition term in $M_{Th}$ and especially in $M_{ADM1}$, the impact of inhibition was assessed by building alternative versions of

**Table 1**
General description of the models designed during the study, separated in two categories: ADM1-like and thermodynamics-based models. The main models of each category ($M_{Th}$ and $M_{ADM1}$) are highlighted with green background.

| | Modification | Growth yield | Inhibition function | Decay rate | $\Delta G_{diss}$ |
|---|---|---|---|---|---|
| ADM1-like ($M_{ADM1}$) models | none | Constant value from ADM1 | Non-competitive inhibition term from ADM1 $I_{H2}$ | Linear expression from ADM1 | – |
| | No decay ($M_{ADM1\_D}$-) | | | Absent | – |
| | No inhibition ($M_{ADM1\_I}$-) | | Absent | Linear expression from ADM1 | – |
| thermodynamics-based models ($M_{Th}$) models | none | Dynamic (calculated using thermodynamics) | Competitive inhibition term calculated using thermodynamics $I_{thermo}$ | Linear expression from ADM1 | Calculated according to ( Heijnen and Kleerebezem, 2010) |
| | No inhibition ($M_{Th\_I}$-) | | Absent | | |
| | Estimate $\Delta G_{diss}$ as a parameter ($M_{Th\_\Delta G}$) | | Competitive inhibition term calculated using thermodynamics $I_{thermo}$ | | Estimated by optimization |

those without the inhibition function (mentioned as $M_{Th\_I}$- and $M_{ADM1\_I}$- respectively for convenience, when comparing to default versions).

In the same way, to test the impact of the decay rate in the $M_{ADM1}$ model, a version of the model without decay has been designed ($M_{ADM1\_D}$-). It is presented in the Supplementary material.

### 2.3. Thermodynamic calculations

The Gibbs energy dissipation method (GEDM) was applied to estimate growth yields (Kleerebezem and Van Loosdrecht, 2010). The Gibbs energies of catabolism ($\Delta G_{cat}$) and anabolism ($\Delta G_{an}$) were calculated as in (Kleerebezem and Van Loosdrecht, 2010):

$$\nu_{s\_1}S_1 + \nu_{s\_2}S_2 + \cdots \nu_{s\_m}S_m = \nu_{p\_1}P_1 + \nu_{p\_2}P_2 + \cdots \nu_{p\_n}P_n$$

$$\Delta G(t) = \Delta G^0 + R \bullet T \bullet log\left(\frac{\prod_i^n P_i(t)^{\nu_{p-i}}}{\prod_i^m S_i(t)^{\nu_{s-i}}}\right) \quad (8)$$

where S are the substrate concentrations of the reaction, P are the product concentrations of the reaction, $\nu_s$ and $\nu_p$ are the stoichiometric coefficients of the products and substrates, respectively, R is the universal gas constant, T is the temperature in K and $\Delta G_0$ is the standard Gibbs free energy of reaction at a given temperature. This approach enabled the calculation of estimates for the energy released from 1 mol of substrate consumed ($\Delta G_{cat}$) and the energy required to synthesize 1 g of biomass ($\Delta G_{an}$).

In order to connect $\Delta G_{cat}$ to $\Delta G_{an}$, dissipated energy ($\Delta G_{diss}$) must also be taken into account (eq.9). The dissipated Gibbs energy ($\Delta G_{diss}$) was calculated using Heijnen's empirical formula (Heijnen and Van Dijken, 1992). Dissipated energy will account for energy that is dissipated as heat during metabolic conversions and energy spent on cell maintenance. According to (Kleerebezem and Van Loosdrecht, 2010), this relation can be presented as:

$\Delta G_{diss} = -\lambda_{cat} \bullet \Delta G_{cat} - \Delta G_{an}$ (9).

$\lambda_{cat}$ is a parameter that shows how many times a catabolic reaction must be carried out to achieve one anabolic reaction. $\Delta G_{diss}$ can be estimated according to (Heijnen and Van Dijken, 1992). However, Heijnen's empirical formula by which $\Delta G_{diss}$ is calculated was estimated using measurements of mostly aerobic microorganisms. To assess the impact of this approximation, similar to (Leurent and Moscoviz, 2022) we also tried to estimate $\Delta G_{diss}$ alongside kinetic parameters ($k_m$, $K_s$) as an additional parameter, in the $M_{Th}$ model (for convenience, mentioned $M_{Th\_\Delta G}$ when comparing parameters, although the model structure is the same as in $M_{Th}$). This approach enabled evaluation of whether $\Delta G_{diss}$ is identifiable from the data and consistent with estimated values.

From eq. 9, $\lambda_{cat,}$ can be calculated for each time point as presented in eq. (10), and used to determine growth yields and stoichiometric coefficients (see Supplementary material for formulas).

$$\lambda_{cat}(t) = \frac{\Delta G_{an}(t) + \Delta G_{diss}}{-\Delta G_{cat}(t)} \quad (10)$$

### 2.4. Inhibition function

Hydrogen accumulation has inhibitory effects on microorganisms oxidizing VFA (in this case SPOB and SAOB) as it makes oxidation of VFA thermodynamically unfavorable. This product inhibition can reduce both substrate uptake and growth rates. In order to account for this thermodynamic constraint, an inhibition function depending on the hydrogen concentration was added as in ADM1 (IWA Task Group for Mathematical Modelling of Anaerobic Digestion Processes, 2005).

In the model similar to classical ADM1 ($M_{ADM1}$), the inhibition function was applied to the uptake rate of SPOB and SAOB, based on $H_2$ accumulation:

$$I_{H_2} = \frac{1}{1 + \frac{[H_2]}{K_{iH_2}}} \quad (11)$$

where $[H_2]$ is the hydrogen concentration in the liquid phase and $K_{iH2}$ is the inhibition constant, defined as the $H_2$ concentration at which the substrate consumption rate of the syntrophic bacteria is inhibited by half.

In model with thermodynamics ($M_{Th}$), the inhibition function was implemented following the approach proposed by Leurent and Moscoviz (Leurent and Moscoviz, 2022) based on the theoretical framework introduced by Jin and Bethke (Jin and Bethke, 2007). In this formulation, the inhibition function depends on both $\Delta G_{diss}$ and $\lambda_{cat}$.

$$I_{thermo} = 1 - exp\left(\frac{-\Delta G_{diss}}{\lambda_{cat} \bullet R \bullet T}\right) \quad (12)$$

The thermodynamic inhibition $I_{thermo}$ is considered competitive, as the dissipative energy used in its calculation explicitly accounts for the reactions that metabolize the substrates to which the inhibition applies. By contrast, the ADM1 inhibition $I_{H2}$ is said to be non-competitive, since the inhibition of uptake is computed from an indirect phenomenological link between hydrogen concentration and uptake rates.

In this formulation, the inhibition function will be activated when the value of $\Delta G_{cat}$ approaches 0 kJ/mol. But according to the literature (Adams et al., 2006; Schink, 1997; Scholten and Conrad, 2000), the catabolic reaction is required to have at least $\Delta G_{cat}$ between −10 to −20 kJ/mol to be implemented by microorganisms and not 0 kJ/mol. To test if this assumption is applicable for our model, the inhibition function was set to start affecting from −10, −12 and −15 kJ/mol. This was done by adding the chosen value to the value of $\Delta G_{cat}$ when calculating $\lambda_{cat}$. As can be seen from equations (11) and (12) inhibition term can have values between 0 and 1. High inhibition corresponds to values of the inhibition factor (I) approaching 0, whereas weak inhibition corresponds to values approaching 1.

### 2.5. Parameter estimation and validation

Following the experiments conducted, $M_{ADM1}$ and $M_{Th}$ models were implemented in CSTR and batch versions. In model $M_{ADM1}$, where the classical ADM1 inhibition function was implemented, eight kinetic parameters were estimated ($k_{m\_HM}$, $K_{s\_HM}$, $k_{m\_SAOB}$, $K_{s\_SAOB}$, $K_{i\_SAOB}$, $k_{m\_SPOB}$, $K_{s\_SPOB}$, $K_{i\_SPOB,}$ (see in Supplementary material for parameter description). Here $k_m$ is maximum uptake rate of substrate, and $K_s$ is half saturation constant. Growth yield values for SPOB and HM were set to default ADM1 values under thermophilic conditions. Growth yield value for SAOB was estimated from Rivera-Salvador *et al.*(Rivera-Salvador et al., 2014). In contrast, to $M_{ADM1}$ the thermodynamic-based model ($M_{Th}$) does not require the estimate of $K_i$, leaving six parameters to be estimated ($k_{m\_HM}$, $K_{s\_HM}$, $k_{m\_SAOB}$, $K_{s\_SAOB}$, $k_{m\_SPOB}$, $K_{s\_SPOB}$). In thermodynamic-based models, growth yield values were calculated using the GEDM. But $M_{Th}$ was also tested, where $\Delta G_{diss}$ values were also optimized for each microorganism, representing three additional parameters to be estimated (mentioned $M_{Th\_\Delta G,}$ to differentiate from $M_{Th}$). This led to a total of nine estimated parameters for $M_{Th\_\Delta G}$ but allowed the model to operate without relying on the empirical GEDM formula for $\Delta G_{diss}$. Besides kinetic parameters, all models require estimation of the initial biomass concentrations for the three microbial groups ($X_{HM}$, $X_{SPOB}$, $X_{SAOB}$).

To estimate model parameters and explore their distribution, we designed a specific strategy in order to make the most of the data available from five different experimental setups (see Fig. 1 and "Experimental data" section). A five-step sequential strategy was implemented to fit the parameters on the most adapted data set and to validate them on external datasets, unseen by previous fitting procedures.

***Step 1.*** Kinetic parameters of SAOB and HM were fitted on the $CSTR_{AC}$ dataset, following a Monte-Carlo approach embedded in an iterative procedure. Namely, initial biomass concentrations (not measured in the dataset) were first randomly chosen. Based on these biomass initial conditions, the kinetic parameters were then optimized, using the least_squared function from the Scipy package (Virtanen et al., 2020). During this and the next steps for optimization, the by the sum of normalized root mean squared errors (NRMSE) of propionate concentration, acetate concentration, and $H_2$ partial pressure, depending on data availability (e.g., only acetate concentration for this step) was used as cost function. Then, the steady-state biomass concentrations obtained with the current optimal parameters were used as new initial conditions for the next optimization step. This iterative cycle was repeated until convergence of both the kinetic parameters and initial biomass values, typically within 10 iterations. We empirically observed that in about 30% of the cases of optimization cycles, during first optimization cycle, it fails and the optimization procedure breaks. We then repeated this procedure 140 times, in order to obtain at least 100 parameter sets, after rejection of unconverged cases. As a result, different parameter sets were obtained for each model and its modifications ($M_{Th}$ = 132, $M_{ADM1}$ = 125, $M_{Th\_I}$-=130, $M_{Th\_\Delta G}$ = 121, $M_{ADM1\_I}$-=106, $M_{ADM1\_D}$-=135). Fitting on CSTR data allowed us to estimate at the same time kinetic parameters without estimating initial concentrations of biomasses as separate parameters.

***Step 2.*** The parameter sets were selected on the $B_{Ac\_Ac}$ dataset. For each parameter set obtained at step 1, we estimated initial biomass, not measured in the dataset, using the dual_annealing global optimization algorithm from the Scipy package (Virtanen et al., 2020) over acetate and $H_2$ data. Estimation of initial biomass helped to fit the model prediction at the initial phase of experimental data, when a lag phase was present. Ideally, biomass concentrations at the start of batch experiments would have been the same as at the end of the CSTR from which it was inoculated. However, as there was a cell material sedimentation in continuous reactors, which was not transferred with the medium to the batches. Because of this, biomass at the end of CSTR experiments may not be the same as at the start of batch experiments. Therefore, the initial concentration of biomass in batch experiments was estimated by optimization. As a criterion to select the best parameters threshold value of the sum of NRMSE (0.28) was used. The threshold value was selected as such, that allowed to select the top 10 parameters from $M_{Th}$ model. Here, the availability of gas-phase data (hydrogen and methane) allowed better discrimination among parameter sets.

***Step 3.*** Selected parameters ($M_{ADM1}$: 12 parameter sets, $M_{Th}$: 10, $M_{ADM1\_D}$-: 20, $M_{Th\_I}$-: 3, $M_{Th\_\Delta G}$: 10) were validated on the external $B_{Prop\_Ac}$ dataset after initial biomass optimization with dual annealing (Virtanen et al., 2020).

***Step 4.*** For each element of the selected parameters selected at Step 2, the kinetic parameters of SPOB were fitted on the $CSTR_{Prop}$ dataset, keeping fixed SAOB and HM parameters, with the same procedure as in Step 1 (one repetition of the iterative process). It was assumed that the kinetic parameters estimated for SAOB and HM in the acetate-fed cultures would remain valid when applied to the more complex propionate-fed systems. This assumption allowed for a reduction in the number of parameters to be fitted, thereby minimizing potential cofounding effects. This assumption was validated, as both models accurately reproduced the dynamics observed in the $CSTR_{Prop}$ and $B_{Prop\_Prop}$ datasets without re-estimating SAOB and HM parameters (Fig. 2).

***Step 5.*** The complete parameter sets (including SAOB, HM and SPOB) were validated on the separate $B_{Prop\_Prop}$ dataset, after optimization of the initial biomass by dual annealing, as in step 3.

Through this, we obtained a complete estimation procedure, including fitting on the most adapted dataset and validation on totally external data, unseen by previous estimations.

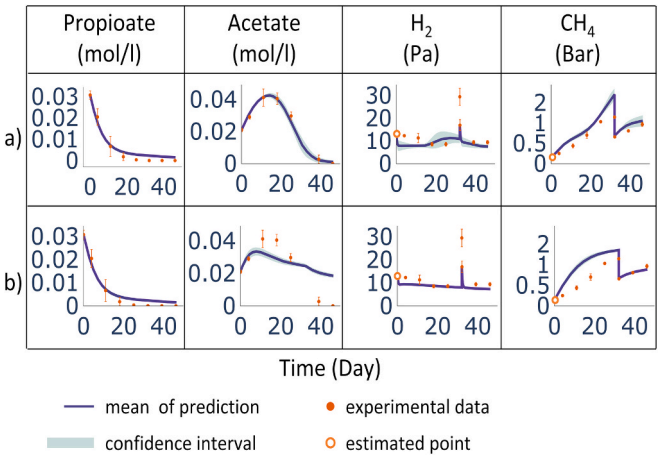


**Fig. 2.** Predictions of $B_{Prop\_Prop}$ batch reactor experiment with $M_{ADM1}$ models using validated parameters. The solid line shows the mean of predictions of all validated parameters, and the highlighted area around it is the confidence interval. Dots indicate the mean of experimental measurements from two reactors, and error bars show the minimum and maximum values. Estimated points (hollow dots) are missing data that were estimated by data imputation using interpolation. $\Delta G_{cat}$ shows the change in available catabolic energy due to the consumption of compounds. Dashed lines indicate levels $\Delta G_{cat}$ of 0 and −15 kJ/mol (i.e. respectively thermodynamic feasibility and minimum energy quantity to sustain ATP synthesis). Inhibition shows the value of the inhibition function of compound consumption, ranging from 1 (no inhibition) to 0 (complete inhibition).

### 2.6. Model implementation

Models were implemented using Python 3.11.5. Integration was carried out with the odeint function from the Scipy library version 1.12.0 (Virtanen et al., 2020). Model goodness of fit (GOF) was assessed by calculating the mean absolute error (MAE) using the mean_absolute_error function with "raw_values" parameter, from Scikit-learn library version 1.7.1 (Pedregosa et al., 2011). In batch experiments, manual gas release from headspace was simulated by dividing the simulation time window into two phases: before gas release and after gas release. Total gas partial pressure, and methane and $CO_2$ percentage in it were measured before and after gas release. It was assumed that the gas mixture was homogeneous, so the gas proportions before and after release were the same, and based on this, the amount of $H_2$ partial pressure was estimated. The partial pressure of the gases after gas release was used as the initial value for the second simulation. Parameter correlations were estimated by corrcoef function from Numpy package version 1.26.2. Scripts and data are freely accessible (see "Data availability").

## 3. Results and discussion

### 3.1. Model without thermodynamics

In the present study, the first analysis assessed the ADM1-based model ($M_{ADM1}$) for its capacity to describe performance data previously obtained from enrichment cultivation of syntrophic acetate and propionate oxidation in the thermophilic, high-ammonia system (Singh et al., 2023). The results demonstrated that goodness of fit (GOF) of the $M_{ADM1}$ model performance on validation data from $B_{Prop\_Ac}$ and $B_{Prop\_Prop}$ experiments was good (see in Supplementary Material), where the most significant error being in $H_2$ partial pressure predictions.

The idea of optimizing a subset of the parameters on dedicated independent datasets is known and accepted approach (Batstone et al., 2003; Rieger et al., 2012). The kinetic parameters of propionate and acetate oxidation were estimated first, and next parameters for butyrate

and valerate production were estimated separately on dedicated data. While estimating parameters on data from a batch reactor and validating them on a continuous reactor is a more common practice (23,39), we opted for the reverse strategy. This allowed us to estimate the biomass steady-state with the iterative procedure of step 1. Conversely, if parameters were to be optimized on batch data, it would have been needed to estimate kinetic parameters alongside with initial concentration of biomass at the same time. It is worth being aware that some authors consider batch experiments not to be ideal representatives of continuous systems such as (Baltes et al., 1994), as estimated parameters in batch can fail to work in continuous conditions.

The distribution of validated parameters for model $M_{ADM1}$ is

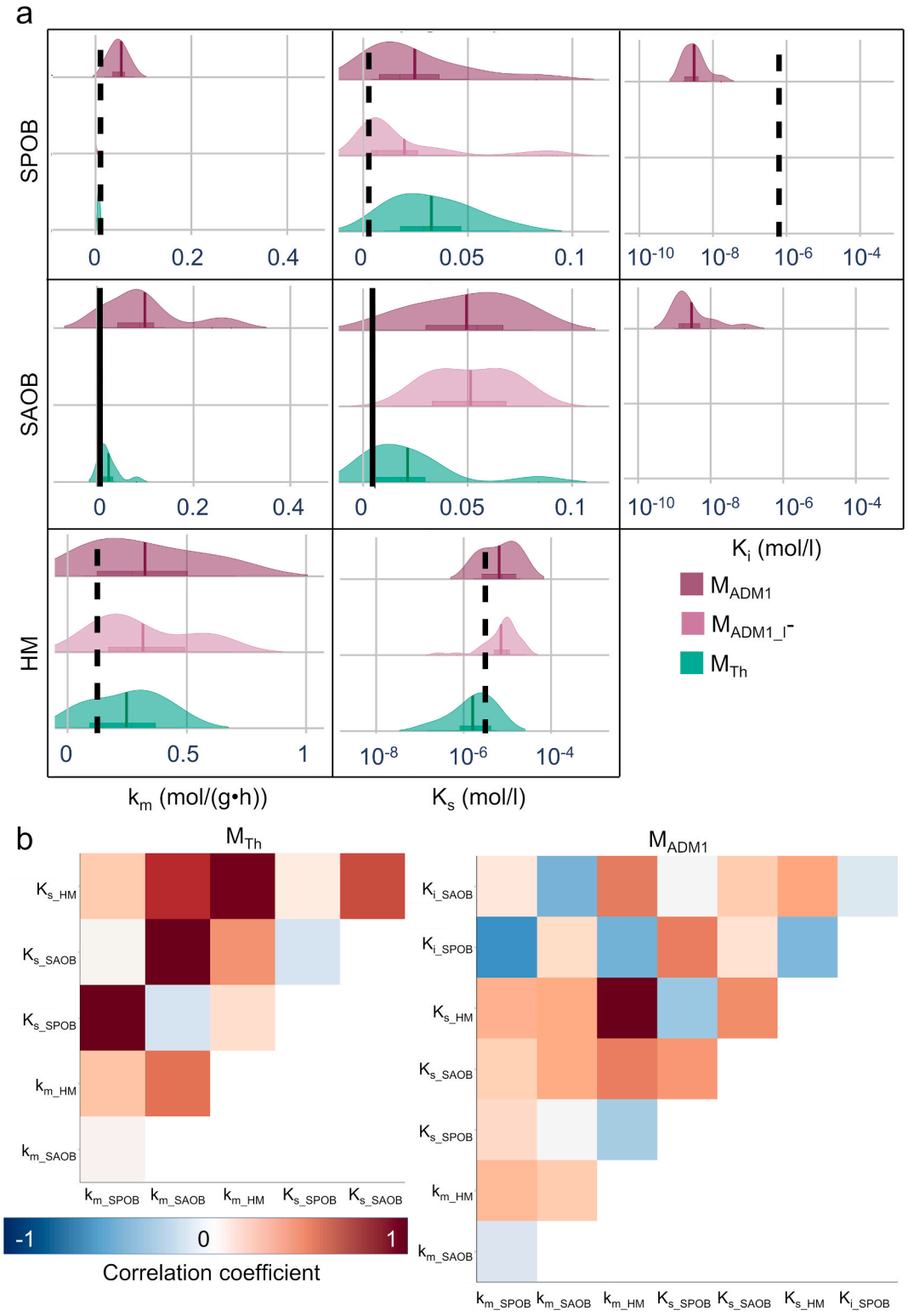


**Fig. 3.** A) distribution of validated parameters. the dash line shows the default value of at thermophile condition in adm1 (IWA, 2005) (if present) and solid line the estimated value from (Rivera-Salvador et al., 2014). b) Co-variance matrix of the validated parameters of the $M_{Th}$ and $M_{ADM1}$ models, at the end of the stepwise procedure.

presented in Fig. 3a. For hydrogenotrophic methanogens the estimated parameters were $k_{m\_HM} = 0.32 \pm 0.22$ mol/(g•h) and $K_{s\_HM} = 9.4 \bullet 10^{-6} \pm 6.9 \bullet 10^{-6}$ mol/l in $M_{ADM1}$. Although spanning a broad range, the estimates remained consistent with ADM1 default values for thermophilic digestion ($k_{m\_HM} = 0.12$ mol/(g•h) and $K_{s\_HM} = 3.13 \bullet 10^{-6}$ mol/l). Parameter estimates for syntrophic propionate-oxidizing bacteria (SPOB) were $k_{m\_SPOB} = 0.047 \pm 0.018$ mol/(g•h) and $K_{s\_SPOB} = 0.025 \pm 0.023$ mol/l in $M_{ADM1}$ (default ADM1 values $k_{m\_SPOB} = 0.01$ mol/(g•h), $K_{s\_SPOB} = 0.0027$ mol/l). The inhibition constant $K_{i\_SPOB}$ was estimated at $4.2 \bullet 10^{-9} \pm 4.06 \bullet 10^{-9}$ mol/l, which is more than two orders of magnitude lower than the default value of ADM1 ($K_{i\_SPOB} = 6.25 \bullet 10^{-7}$ mol/l). Such a low $K_{i\_SPOB}$ value mathematically implies strong inhibition under nearly all tested conditions. In practice, the inhibition term remained close to zero and essentially constant throughout the batch simulations (Fig. 2), indicating that it did influence the results, but did not contribute to explaining the observed dynamics of substrates and products. For syntrophic acetate-oxidizing bacteria (SAOB), parameter estimates were distributed over a wide range, similar to those of SPOB, with $k_{m\_SAOB} = 0.1 \pm 0.08$ mol/(g•h) and $K_{s\_SAOB} = 0.05 \pm 0.022$ mol/l for $M_{ADM1}$. Direct comparison with ADM1 parameters was not possible, since SAOB are not included in the original model. However, when compared to literature data, these estimated values are generally higher than those reported ($k_{m\_SAOB}$ = 0.001–0.006 mol/(g•h), $K_{s\_SAOB}$ = 0.002–0.004 mol/l (Capson-Tojo et al., 2021; Montecchio et al., 2017; Rivera-Salvador et al., 2014)). Similarly, the inhibition constant $K_{i\_SAOB}$ was estimated at an unrealistically low value ($K_{i\_SAOB} = 1.02 \bullet 10^{-8} \pm 2{,}38 \bullet 10^{-8}$ mol/l), resulting in a nearly constant, close to zero inhibition term (meaning strong inhibition) throughout the batch simulations.

The wide ranges of parameter estimates obtained with the ADM1-based model $M_{ADM1}$ (Fig. 3a), suggested a poor parameter identifiability. To better understand the origin of this uncertainty, we examined pairwise parameter correlations (Fig. 3b, model $M_{ADM1}$). The analysis of parameter correlations shows that $k_{m\_HM}$ and $K_{s\_HM}$ parameters are positively correlated for hydrogenotrophic methanogens (HM). This reflects a structural identifiability limitation: because substrate concentrations remain below $K_{s\_HM}$ for most of the experimental time, only the $k_{m\_HM}/K_{s\_HM}$ ratio is effectively constrained by the data. Such correlations are common in Monod-based models and highlight the need for complementary data (e.g., experiments at higher substrate concentration) to resolve individual kinetic parameters. For SAOB and SPOB, the correlation is weaker, likely due to interferences from the additional inhibition constant parameters $K_{i\_SAOB}$ and $K_{i\_SPOB}$. Indeed, for these groups, a strong negative correlation is observed between $k_m$ and $K_i$, suggesting that the model fitting process allows high uptake rates to be compensated by strong inhibition. Such parameter compensation explains the broad and elevated $k_m$ values obtained for these groups, as well as the unrealistically low $K_i$ estimates discussed above.

According to the optimal experimental design approach (Baltes et al., 1994), it is impossible to uniquely estimate the parameters of the simple Monod equation from batch experiments. Kinetic parameters can be estimated with more than one operating condition tested in CSTR. With experimental data at more than one dilution rate tested in the same CSTR, the model would likely explore a wider range of substrate consumption rates, and the kinetic parameters could be more reliably identified. This is illustrated by the analysis results presented in Supplementary Material, where the growth rate of SAOB is plotted against the acetate concentration. We can see that growth rates calculated from different parameters are similar to each other at the concentrations explored in $CSTR_{Ac}$ close to steady state but differ substantially at higher concentrations of steady state. This phenomenon was, for example, analyzed by Bernard *et al.* in the modeling of an anaerobic wastewater treatment process (Bernard et al., 2001). The prediction of different parameter sets, which were similar in the case of the initial dilution rate, start to differentiate under the second dilution rate. The same can also be achieved with substrate pulses during one dilution rate, as discussed by Donoso-Bravo *et al.* (Donoso-Bravo et al., 2011). The lack of biomass information also has a major impact, as a change in the substrate-to-biomass ratio can change the correlation of Monod parameters (Raposo et al., 2009). Here, initial biomass was estimated by optimization, which is a common practice, but the measurement of biomass by measurements is always preferable (Donoso-Bravo et al., 2011). However, estimating the individual biomass of complex cultures, as in our case, is technically difficult. Singh et al. 2023, quantified the abundance of HM (Methanomicrobiales and Methanobacteriales) in reactors using qPCR. Based on this data, we calculated the total methanogen biomass in batch reactors (see Supplementary Material). Comparison with methanogen biomass predicted by $M_{ADM1}$ shows that the estimated and predicted values are of the same order of magnitude, indicating that the optimization-based estimates provide a reasonable approximation of experimental observations.

These first results highlight a parameter identifiability problem, preventing a reliable estimation of the syntrophs' kinetic parameters. This issue arises partly from the limited diversity of the experimental data (e.g., insufficient range of dilution rates and substrate concentrations), and partly from structural constraints of the $M_{ADM1}$ model, with excessive degrees of freedom and inadequate inhibition dynamics.

### 3.2. Impact of model structure on parameter distributions and model outcome

To further explore the impact of model structure on parameters, an additional model was evaluated, representing a modified version of the ADM1-based $M_{ADM1}$ model without the inhibition function. The development of this model, denoted $M_{ADM1\_I}$-, was motivated by the observation that the value of the inhibition function in the $M_{ADM1}$ model remained nearly constant throughout most experiments, even in batch conditions before the substrate was completely consumed (Fig. 2). This behavior reflects the relatively stable hydrogen partial pressures measured during the experiments, which limited the variation of the inhibition term during the simulated periods. Additionally, due to the very low $K_i$ parameters, both SAOB and SPOB were predicted to be strongly inhibited at all times and the maximum uptake rates for SAOB and SPOB were thus overestimated, as discussed above. Simulations with $M_{ADM1\_I}$- (see in Supplementary Material) were nearly identical to those of their parent models, as can be seen on the tables presented in Supplementary Material. Despite similar predictive performance, notable differences were observed in parameter distributions between $M_{ADM1\_I}$- and $M_{ADM1}$ (Fig. 3a), particularly for the maximum uptake rates $k_{m\_SPOB} = 0{,}0013 \pm 0.0008$ mol/(g•h) and $k_{m\_SAOB} = 0{,}0019 \pm 0{,}0005$ mol/(g•h). The distribution of the $k_{m\_SPOB}$ value was lower compared to the default value of ADM1 ($k_{m\_SPOB} = 0.01$ mol/(g · h)) and showed no overlap with it. Distributions of $k_m$ parameters were significantly narrower than in $M_{ADM1}$ (Fig. 3a). Other parameters have a similar distribution as in $M_{ADM1}$ ($k_{m\_HM} = 0.31 \pm 0.19$, $K_{s\_SPOB} = 0{,}0198 \pm 0{,}0264$, $K_{s\_SAOB} = 0{,}0513 \pm 0{,}019$, $K_{s\_HM} = 9{,}84 \bullet 10^{-6} \pm 6{,}53 \bullet 10^{-6}$). The narrower distribution of $k_m$ parameters confirms that the inclusion of the empirical inhibition parameters $K_i$ in $M_{ADM1}$ introduced compensatory effects with $k_m$, thereby reducing the identifiability of parameters. By contrast, in model $M_{ADM1\_I}$- where inhibition was removed, these compensations are avoided, leading to tighter and more robust parameter estimates. In other words, microorganisms in $M_{ADM1\_I}$- are not inhibited and display a lower maximum uptake rate, which seems to be a more realistic prediction. This raises the question of whether the inhibition function is necessary in the model. In our case, the absence of inhibition is likely explained by the efficient consumption of $H_2$ by hydrogenotrophic methanogens, which prevents $H_2$ from reaching inhibitory concentrations. Nevertheless, removing inhibition term may reduce the predictive capacity of the model in scenarios where $H_2$ accumulation becomes significant.

As mentioned above, the values of maximum uptake rate $k_{m\_SPOB}$ identified with $M_{ADM1\_I}$- are significantly lower than the ADM1 default value, suggesting that propionate oxidizers in these experiments have a

low maximum uptake rate. This finding is not surprising, as syntrophs were growing under harsh conditions (limited energy, high ammonia concentration, etc.). Nevertheless, the estimated $k_{m\_SPOB}$ values remain within the range reported in the literature ($8.33 \bullet 10^{-5}$ – 0.0168 mol/(g•h) (Leurent and Moscoviz, 2022)). However, this range is notably wide and thus offers limited guidance for parameter estimation. A possible source of difficulty in the estimation of the maximum uptake rate lies in the uncertainty of the growth yield values. During model calibration, it is not the uptake rate itself that is directly constrained by the data, but rather the product of the uptake rate and growth yield, *i.e.* the growth rate. Consequently, overestimating the growth yield necessarily leads to an underestimation of the maximum uptake rate and conversely. In $M_{ADM1}$ and $M_{ADM1\_I}$-, the growth yields of SPOB and HM were assumed to be the ADM1 default values in thermophilic conditions, while the growth yield of SAOB was taken from the literature (Rivera-Salvador et al., 2014). However, experimental studies in batch reactors (Scholten and Conrad, 2000) suggest that ADM1 default values for SPOB and HM are likely overestimated (see more in "Thermodynamic estimation of microbial growth yields").

### 3.3. Model with thermodynamics

In a similar experimental setup, the advantages of the model with thermodynamics were already demonstrated by (Leurent and Moscoviz, 2022). It introduces a different inhibition term calculated from thermodynamics without introducing additional parameters (see section "Inhibition function"). This implies that the introduction of thermodynamics can help to avoid the limitations of previous models related to inhibition function. Also, as mentioned before, in this approach, growth yield (see section "Thermodynamic calculations") was also estimated from thermodynamics. As a result, this approach is expected to provide more realistic growth yields and to enforce the thermodynamic feasibility of reactions as a function of hydrogen partial pressure (and concentrations of other compounds), without introducing additional parameters. Following this, a version of the model with thermodynamics ($M_{Th}$) was constructed.

The model with thermodynamics $M_{Th}$ performed similarly to previous models on validation data (see in Supplementary Material), indicating good fitting. Parameters estimated for hydrogenotrophic methanogens (HM) were $k_{m\_HM} = 0.25 \pm 0.14$ mol/(g•h) and $K_{s\_HM} = 2.5 \bullet 10^{-6} \pm 1.9 \bullet 10^{-6}$ mol/l (Fig. 3a). Similarly to $M_{ADM1}$, these parameters spanned relatively wide ranges but remained consistent with ADM1 default parameters for thermophilic anaerobic digestion ($k_{m\_HM} = 0.12$ mol/(g•h) and $K_{s\_HM} = 3.13 \bullet 10^{-6}$ mol/l). Parameters estimated for SPOB were $k_{m\_SPOB} = 0.007 \pm 0.002$ mol/(g•h) and $K_{s\_SPOB} = 0.033 \pm 0.018$ mol/l. In $M_{Th}$, the distribution of $k_{m\_SPOB}$ was narrower and centered around values close to ADM1 parameters ($k_{m\_SPOB} = 0.01$ mol/(g•h)) compared to $M_{ADM1}$ and $M_{ADM1\_I}$-. For SAOB, estimated parameters were $k_{m\_SAOB} = 0.024 \pm 0.021$ mol/(g•h) and $K_{s\_SAOB} = 0.021 \pm 0.022$ mol/l, with values generally higher than those reported ($k_{m\_SAOB}$ = 0.001–0.006, $K_{s\_SAOB}$ = 0.002–0.004 (Capson-Tojo et al., 2021; Montecchio et al., 2017; Rivera-Salvador et al., 2014)). $M_{Th}$ benefited from the reduced number of parameters, as thermodynamic constraints eliminated the need to estimate the empirical inhibition constant $K_i$, since inhibition emerges directly from the energetic feasibility of substrate consumption. As a result, $k_m$ parameters for SAOB and SPOB show narrower distributions than in $M_{ADM1}$ model, comparable to distributions obtained with $M_{ADM1\_I}$- model. Nevertheless, $K_s$ parameters in $M_{Th}$ remained broadly distributed and correlated to $k_m$ (Fig. 3b) reflecting the limitations of experimental data as discussed above.

In syntrophic metabolism, thermodynamic feasibility is a critical constraint: the oxidation of substrates like propionate or acetate becomes energetically unfavorable when hydrogen partial pressure is too high. The classic ADM1 inhibition function (equation (11) implemented in $M_{ADM1}$ is supposed to represent this limitation by reducing the uptake rate of syntrophic oxidizers (SPOB and SAOB) at high $H_2$ concentrations. However, this regulatory term is phenomenological and does not explicitly avoid thermodynamically infeasible situations. Indeed, with the $M_{ADM1}$ model, several situations arise where reactions are predicted to proceed despite violating the second law of thermodynamics (*i.e.* with positive $\Delta G_{cat}$). Moreover, this inhibition is applied only to SPOB and SAOB, not to HM, which are also subject to thermodynamic limitations. This is illustrated in batch reactor simulations, where $M_{ADM1}$ predicts complete consumption of $H_2$ by the end of cultivation (Fig. 2), even though the $\Delta G_{cat}$ of hydrogenotrophic methanogenesis becomes positive as the $H_2$ partial pressure decreases. In contrast, the thermodynamic inhibition function implemented in $M_{Th}$ explicitly prevents reactions from proceeding when catabolic energy becomes insufficient. This applies equally to all microbial groups, including HM, without the need to introduce additional inhibition parameters. This leads, for example, to the prediction of a residual $H_2$ partial pressure of 2.3 Pa at the end of batch experiments, more in line with the experimental data (Fig. 4). The mathematical behavior of the thermodynamic function, with a sharp transition from maximum rate to complete inhibition (inhibition term value $\approx 0$) near $\Delta G_{cat} = 0$ (Leurent and Moscoviz, 2022), ensures that reactions only proceed when thermodynamically allowed, while the smoother function of ADM1 is less appropriate in conditions near thermodynamic limits (Leurent and Moscoviz, 2022). It is however important to note that syntrophs may utilize alternative electron carriers, such as formate, or other mechanisms such as direct interspecies electron transfer (see section 3.4), which are not included in the current models.

As discussed by Patón and Rodríguez (Patón and Rodríguez, 2019a), the strict enforcement of thermodynamic feasibility is not always considered essential if the model remains predictive at the reactor scale. However, the present case highlights a situation where the empirical inhibition function used in ADM1 is not only imprecise but also potentially counterproductive. In our dataset, H2 partial pressure fluctuation did not reflect any fluctuations in propionate or acetate consumption, which in turn shows that syntrophs are not inhibited by it. Or to say it differently, H2 is not in the range to cause inhibition. This condition makes the calibration of the inhibition constant Ki difficult. As a result, the $M_{ADM1}$ model predicts a persistent, moderate inhibition even when it is not thermodynamically justified (see Fig. 2). Thus, introducing the inhibition parameter $K_i$ increases the model complexity without improving its descriptive or predictive power. This is reflected in the broader and less identifiable parameter distributions observed for the $M_{ADM1}$ model, as discussed above. In contrast, the thermodynamic inhibition in $M_{Th}$ does not require additional parameters; it emerges from first principles and leads to more constrained and interpretable parameter estimates. The thermodynamic formulation therefore provides both a safeguard against physically unfeasible predictions and a more robust basis for parameter estimation.

In the thermodynamic model $M_{Th}$, growth yields are estimated from catabolic and anabolic energy balances using the Gibbs Energy Dissipation Method (GEDM see Material & Methods and (Kleerebezem and Van Loosdrecht, 2010)). This approach is particularly useful for syntrophic cultures where direct growth yield measurements are difficult. For SPOB and HM, yield values are available from pure cultures (Scholten and Conrad, 2000; Uhlenhut et al., 2018; Wallrabenstein et al., 1994), whereas no direct yield measurements were found for thermophilic SAOB. For the latter, the yield estimate from (Rivera-Salvador et al., 2014), derived using differential evolution algorithms was used as reference. For SPOB, the growth yields ($g_{biomass}/mol_{substrate}$) predicted by the GEDM were lower than those used in $M_{ADM1}$ or ADM1, but in better agreement with literature data. For instance, the average predicted yield for SPOB was 0.92 g/mol in batch (vs. 1.02 g/mol measured (Scholten and Conrad, 2000)), and 0.95 g/mol in CSTR (vs. 1.4–1.69 g/mol reported (Scholten and Conrad, 2000)), while ADM1 and $M_{ADM1}$ assume much higher yields values (4.09 g/mol in thermophilic conditions and 3.27 g/mol in mesophilic conditions). For HM, the average predicted growth yields were 0.29 g/mol in batch (vs. 0.18 g/mol measured (Scholten and Conrad, 2000)) and 0.39 g/mol in CSTR

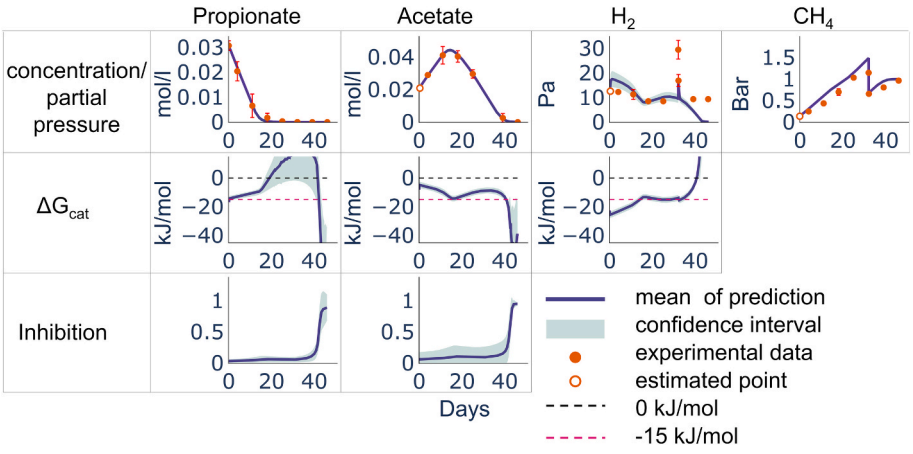


**Fig. 4.** Predictions of $B_{Prop\_Prop}$ batch reactor experiment with $M_{Th}$ model using validated parameters. The solid line shows the mean of predictions of all validated parameters, and the highlighted area around it is the confidence interval. Dots indicate the mean of experimental measurements from two reactors, and error bars show the minimum and maximum values. Estimated points (hollow dots) are missing data that were estimated by data imputation using interpolation. $\Delta G_{cat}$ shows the change in available catabolic energy due to the consumption of compounds. Dashed lines indicate levels $\Delta G_{cat}$ of 0 and −15 kJ/mol (i.e. respectively thermodynamic feasibility and minimum energy quantity to sustain ATP synthesis). Inhibition shows the value of the inhibition function of compound consumption, ranging from 1 (no inhibition) to 0 (complete inhibition).

(vs. 0.98–1.4 g/mol reported (Scholten and Conrad, 2000)), compared to 0.7 g/mol in ADM1. As for SPOB, GEDM values for HM are closer to experimental data than default ADM1 values. It should be noted that these microorganisms grow in stress conditions which require additional ATP investment for maintenance and stress response, potentially reducing the actual growth yield even further. Predictions of yield are closer to experimental values from batch experiments than from CSTR. Although both the model and experiments show higher growth yield in CSTR experiments than in batch, the increase is smaller in model predictions. For SAOB, the average predicted growth yield was 0.64 g/mol in batch and 0.231 g/mol in CSTR. Although $\Delta G_{cat}$ of SAOB was lower than that of HM, its lower $\Delta G_{diss}$ (415 kJ/mol) led to higher yields than in HM. The predicted total methanogen biomass is very close to the values estimated from qPCR and even closer than the $M_{ADM1}$ predictions. This further highlights the utility and accuracy of GEDM method to estimate yields of these microorganisms.

In an attempt to refine the prediction of growth yields using the GEDM, $\Delta G_{diss}$ was treated as a free parameter in $M_{Th}$ (mentioned as $M_{Th\_\Delta G}$) and estimated with kinetic parameters. This modification did not significantly improve model performance. The estimated values of $\Delta G_{diss}$ showed a broad distribution across parameter sets (see in Supplementary Material), indicating that it cannot be reliably constrained with the current data. These findings highlight the need for targeted experimental studies on hydrogenotrophic methanogens in chemostat cultures to accurately quantify their maximum growth yields and maintenance coefficients. Such measurements would strengthen the empirical basis of the GEDM and help refine $\Delta G_{diss}$ estimates, improving the predictive accuracy of thermodynamic models for syntrophic communities.

As previously mentioned, growth yields estimated using GEDM in our study yielded values that are generally lower than experimental values from pure cultures for SPOB (underestimation by 10–40%), but they are much closer to literature data than those reported by Patón and Rodríguez using the GEDM (Patón and Rodríguez, 2019b). In their *meta*-analysis, GEDM systematically underestimated the yield of SPOB by 64–88% compared to experimental values. The discrepancy is due to differences in how $p(H_2)$ values were treated. In their *meta*-analysis, thermodynamic calculations were performed using available data from the literature, which often lacked precise measurements of $H_2$ partial pressure or concentration. As a result, they had to make assumptions on $p(H_2)$ values, which may have led to an underestimation of the actual $\Delta G_{cat}$. In our case, the thermodynamic feasibility is dynamically computed from the simulated $p(H_2)$, which was itself calibrated to match experimental observations. This results in more realistic $\Delta G_{cat}$ values and demonstrates that the GEDM provides reasonable estimates of SPOB growth yields under the studied conditions. In another study, Patón and Rodríguez also reported lower growth yield when incorporating thermodynamics into ADM1 (Patón and Rodríguez, 2019a), which resulted in the accumulation of propionate in their model predictions. However, as highlighted by Leurent and Moscoviz (Leurent and Moscoviz, 2022), this outcome was largely due to the fact that all other parameters were kept unchanged, despite altered energy constraints. Syntrophic metabolism operates very close to thermodynamic equilibrium, making model predictions highly sensitive to the actual concentrations and partial pressures of key metabolites, particularly $H_2$. Accurate simulation of syntrophic processes therefore requires not only thermodynamically consistent formulations but also the most precise possible representation of the physicochemical environment (Scholten and Conrad, 2000). Additionally, as analyzed by Kleerebezem *et al.* (Kleerebezem and Stams, 2000), ADM1-type models may be unable to accurately represent near-equilibrium metabolisms. Indeed, in such conditions, substrate consumption and biomass generation may proceed independently, making their connection via fixed stoichiometric coefficients questionable. This limitation highlights the relevance of using GEDM, which balances anabolic and catabolic energy flows and naturally produces variable growth yields.

### 3.4. Thermodynamic inhibition and biological minimum energy quantum

Beyond the primary benefits expected from including thermodynamic constraints in $M_{Th}$, such as reduced parametrization and the ability to represent a wider range of conditions, the model also provides an opportunity to explore fundamental questions regarding the energetic limits of life. In particular, the concept of biological minimum energy quantum, *i.e.*, the minimal $\Delta G_{cat}$ required to sustain ATP synthesis, can be explicitly tested with $M_{Th}$.

Interestingly, while the thermodynamic formulation in $M_{Th}$ prevents infeasible hydrogen depletion, unlike $M_{ADM1}$, it still tends to underestimate the residual $H_2$ partial pressures at the end of batch experiments compared to experimental observations (see Fig. 2). This discrepancy can be explained by the fact that the thermodynamic inhibition function is triggered only when $\Delta G_{cat}$ approaches zero, *i.e.*, at the strict thermodynamic feasibility limit. However, sustaining ATP synthesis in biological systems is generally thought to require a minimum energy quantum,

with classical estimates around −15 to −20 kJ/mol (Schink, 1997). This value remains debated, and several studies report that microbial growth may occur at $\Delta G_{cat}$ values closer to zero (Adams et al., 2006; Scholten and Conrad, 2000). To evaluate the impact of imposing a biologically meaningful $\Delta G_{cat}$ threshold, the $B_{Prop\_Prop}$ reactor was simulated using the validated parameter sets from $M_{Th}$, but imposing a $\Delta G_{cat}$ threshold of −10, −12, and −15 kJ/mol for all groups: SAOB, SPOB, and HM. At constraint levels of −10 and −12 kJ/mol, the GOF of $H_2$ prediction declined. For propionate, while the constraint of −10 kJ/mol did not change GOF much, the −12 kJ/mol constraint had a more noticeable effect, although it was still small (see in Supplementary Material). Those constraints, however caused a significant mismatch in the predicted acetate dynamics. A test with −15 kJ/mol failed, as the model failed to make any even remotely acceptable prediction. A second test was thus performed, in which the $\Delta G_{cat}$ threshold of −12 kJ/mol was applied only to SPOB and HM, while SAOB were allowed to operate without constraint. This modification led to predictions that closely matched the experimental data, both in terms of residual $H_2$ partial pressure and substrate degradation dynamics (Fig. 5b).

These results suggest that enforcing a biologically meaningful $\Delta G_{cat}$ threshold can improve the accuracy of model predictions, but that a uniform threshold for all groups may be overly restrictive. In particular, SAOB in our system appears to grow with $\Delta G_{cat}$ values close to zero (often above −10 kJ/mol), indicating a potentially specific energy conservation strategy not included in the model. Similarly in literature, high and at times positive $\Delta G_{cat}$ for acetate oxidation was predicted by models in mesophilic cultures operating under high ammonia conditions (Weng et al., 2024; Westerholm et al., 2019, 2018). Such a prediction raises important questions about the metabolic pathways of syntrophs and electron transfer mechanisms. If predicted $\Delta G_{cat}$ values remain unrealistically high while oxidation still proceeds, it may indicate that $H_2$ is not the sole electron carrier. Indeed, previous studies have reported the expression of formate dehydrogenase by both the thermophilic SAOB and the cooperating methanogenic partner, supporting the possibility of formate-based transfer (Singh et al., 2023; Weng et al., 2024). Although $H_2$ diffuses faster than formate, making it an effective carrier at short distances, while formate becomes more advantageous for longer-range transfer (Boone et al., 1989; Gujer and Zehnder, 1983) there is no evidence that nature of electron carrier influenced formation of flocs (Weng et al., 2025). Microorganisms may dynamically switch between $H_2$ and formate, depending on local concentrations and spatial organization within the microbial consortium (Montag and Schink, 2018). In structured aggregates, local metabolite concentrations may differ significantly from bulk measurements. As a result, thermodynamic constraints computed using bulk concentrations may not accurately reflect the actual energetic conditions experienced by microorganisms, potentially leading to biased $\Delta G_{cat}$ estimates and incorrect predictions. However, floc formation appeared limited under the thermophilic conditions of the experiments studied here (from on-going batch experiments). Furthermore, *Acetomicrobium* species using the glycine cleavage pathway were also detected to be active in the thermophilic enrichment cultures (Singh et al., 2023). Based on its functional gene repertoire, this species appeared to possess broad metabolic capabilities and can use different amino acids as substrates. Species with different metabolic capacities have been demonstrated to be involved in syntrophic acetate oxidation (Friedline et al., 2025; Weng et al., 2024), indicating that acetate oxidizers apart from energy gained from syntrophic acetate oxidation can also have alternative source of energy, to cope with energy limitations (Weng et al., 2024).

### 3.5. Perspectives

These results raise important questions regarding electron transfer mechanisms. Under the conditions studied, microorganisms may rely on a combination of H2 and formate transfer, and potentially direct interspecies electron transfer (DIET), to overcome thermodynamic constraints. Additionally, the spatial organization of microbial cells, including the presence of flocs, likely influences local thermodynamic conditions experienced by individual cells, affecting their growth and metabolic activity. These findings suggest several avenues for future research: systematic growth experiments in continuous reactors under varying dilution rates could enable the unique identification of kinetic parameters. Measuring formate concentrations and assessing the potential contribution of DIET would provide a more complete understanding of the thermodynamics governing these processes. Finally, a deeper understanding of the metabolism of these species is needed to evaluate the possible energy-conserving mechanisms they employ for ATP synthesis.

## 4. Conclusions

In this study, we developed and evaluated a thermodynamically-constrained model ($M_{Th}$) for the syntrophic oxidation of volatile fatty acids, extending classical ADM1-based approaches. By deriving growth yields and inhibition functions directly from thermodynamic principles, the model provides several clear advantages. Quantitatively, $M_{Th}$

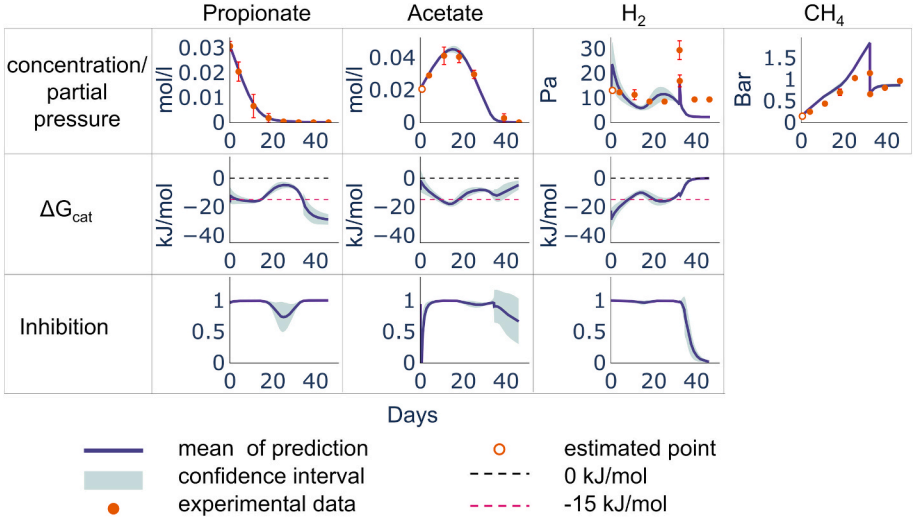


**Fig. 5.** Simulation of $B_{Prop\_Prop}$ experiment with $M_{Th}$ model using validated parameters. a) $\Delta G_{cat}$ of SPOB, SAOB and HM restricted to be lower than −12 instead of 0 kJ/mol. (b) $\Delta G_{cat}$ of SPOB and HM restricted to be lower than −12 instead of 0 kJ/mol.

achieves predictive performance comparable to ADM1 variants across all key metabolites, as measured by mean absolute errors (MAE), while requiring fewer adjustable parameters due to the removal of the empirical inhibition term. This combination of similar predictive accuracy with reduced parameterization demonstrates improved structural parsimony, limiting compensatory effects between parameters and resulting in narrower parameter distributions across repeated multi-start optimizations. Thermodynamic constraints also allowed for the estimation of realistic growth yields, lower than default ADM1 values and closer to experimental observations from defined cultures. The incorporation of a biologically meaningful minimum $\Delta G_{cat}$ further highlighted the energetic limits of syntrophic metabolisms and suggested potential differences in metabolic strategies among functional groups, particularly SAOB. Overall, this work demonstrates that integrating thermodynamic constraints into anaerobic digestion models enhances both predictive accuracy and mechanistic insight. It provides a robust framework for investigating syntrophic interactions, improving parameter identifiability, and creating models that can guide the design and optimization of bioprocesses.

**Declaration of generative AI and AI-assisted technologies in the manuscript preparation process**.

Artificial intelligence tools (ChatGPT) were used exclusively to assist with language editing, including improvement of English style, grammar, and clarity, as well as translation from French to English.

## CRediT authorship contribution statement

**Sahak Yeghiazaryan:** Writing – original draft, Visualization, Investigation. **Gabriel Capson-Tojo:** Writing – review & editing, Methodology. **Jean-Philippe Steyer:** Writing – review & editing, Methodology. **Maria Westerholm:** Writing – review & editing, Resources. **Nicolas Bernet:** Writing – review & editing, Supervision, Conceptualization. **Simon Labarthe:** Writing – review & editing, Supervision, Methodology, Conceptualization. **Elie Desmond-Le Quemener:** Writing – review & editing, Supervision, Methodology, Conceptualization.

## Declaration of competing interest

The authors declare that they have no known competing financial interests or personal relationships that could have appeared to influence the work reported in this paper.

## Acknowledgements

The INRAE MICA division and DIGIT-BIO metaprogramme are gratefully acknowledged for the PhD fellowship allocated to Sahak Yeghiazaryan, and Novo Nordisk Foundation (grant number NNF23OC0081830) is acknowledged for research funding for Maria Westerholm.

## Appendix A. Supplementary data

Supplementary data to this article can be found online at https://doi.org/10.1016/j.biortech.2026.134365.

## Data availability

The scripts and data that support the results of this paper can be accessed here or in the HAL repository by hal-05545645 number.

## References

Adams, C.J., Redmond, M.C., Valentine, D.L., 2006. Pure-Culture growth of Fermentative Bacteria, Facilitated by H2 Removal: Bioenergetics and H2 production. Appl. Environ. Microbiol. 72, 1079–1085. https://doi.org/10.1128/AEM.72.2.1079-1085.2006.

Antonopoulou, G., Gavala, H.N., Skiadas, I.V., Lyberatos, G., 2012. ADM1-based modeling of methane production from acidified sweet sorghum extract in a two stage process. Bioresour. Technol. 106, 10–19. https://doi.org/10.1016/j.biortech.2011.11.088.

Baltes, M., Schneider, R., Sturm, C., Reuss, M., 1994. Optimal Experimental Design for Parameter Estimation in Unstructured Growth Models. Biotechnol. Prog. 10, 480–488. https://doi.org/10.1021/bp00029a005.

Batstone, D.J., Keller, J., Angelidaki, I., Kalyuzhnyi, S.V., Pavlostathis, S.G., Rozzi, A., Sanders, W.T.M., Siegrist, H., Vavilin, V.A., 2002. The IWA Anaerobic Digestion Model No 1 (ADM1). Water Sci. Technol. J. Int. Assoc. Water Pollut. Res. 45, 65–73. https://doi.org/10.2166/wst.2002.0292.

Batstone, D.J., Pind, P.F., Angelidaki, I., 2003. Kinetics of thermophilic, anaerobic oxidation of straight and branched chain butyrate and valerate. Biotechnol. Bioeng. 84, 195–204. https://doi.org/10.1002/bit.10753.

Bernard, O., Hadj-Sadok, Z., Dochain, D., Genovesi, A., Steyer, J.P., 2001. Dynamical model development and parameter identification for an anaerobic wastewater treatment process. Biotechnol. Bioeng. 75, 424–438. https://doi.org/10.1002/bit.10036.

Boone, D.R., Johnson, R.L., Liu, Y., 1989. Diffusion of the Interspecies Electron Carriers H2 and Formate in Methanogenic Ecosystems and its Implications in the Measurement of Km for H2 or Formate Uptake. Appl. Environ. Microbiol. 55, 1735–1741. https://doi.org/10.1128/aem.55.7.1735-1741.1989.

Capson-Tojo, G., Astals, S., Robles, Á., 2021. Considering syntrophic acetate oxidation and ionic strength improves the performance of models for food waste anaerobic digestion. Bioresour. Technol. 341. https://doi.org/10.1016/j.biortech.2021.125802.

Capson-Tojo, G., Moscoviz, R., Astals, S., Robles, Á., Steyer, J.-P., 2020. Unraveling the literature chaos around free ammonia inhibition in anaerobic digestion. Renew. Sustain. Energy Rev. 117. https://doi.org/10.1016/j.rser.2019.109487.

Chen, J.L., Ortiz, R., Steele, T.W.J., Stuckey, D.C., 2014. Toxicants inhibiting anaerobic digestion: a review. Biotechnol. Adv. 32, 1523–1534. https://doi.org/10.1016/j.biotechadv.2014.10.005.

Dolfing, J., 2014. Thermodynamic Constraints on Syntrophic Acetate Oxidation. Appl. Environ. Microbiol. 80, 1539–1541. https://doi.org/10.1128/AEM.03312-13.

Donoso-Bravo, A., Mailier, J., Martin, C., Rodríguez, J., Aceves-Lara, C.A., Wouwer, A.V., 2011. Model selection, identification and validation in anaerobic digestion: a review. Water Res. 45, 5347–5364. https://doi.org/10.1016/j.watres.2011.08.059.

Friedline, S., McDaniel, E.A., Scarborough, M., Madill, M., Waring, K., Lin, V.S., Malmstrom, R.R., Goudeau, D., Chrisler, W., Dueholm, M.K.D., Gorham, L.J., Kombala, C.J., Griggs, L.H., Olson, H.M., Lehmann, S.B., Munoz, N., Trejo, J., Tolic, N., Pasa-Tolic, L., Williams, S.M., Lipton, M., Hallam, S.J., Ziels, R.M., 2025. Activity-targeted metaproteomics uncovers rare syntrophic bacteria central to anaerobic community metabolism. Nat. Microbiol. 10, 2749–2767. https://doi.org/10.1038/s41564-025-02146-w.

Gujer, W., Zehnder, A.J.B., 1983. Conversion Processes in Anaerobic Digestion. Water Sci. Technol. 15, 127–167. https://doi.org/10.2166/wst.1983.0164.

Hattori, S., Luo, H., Shoun, H., Kamagata, Y., 2001. Involvement of formate as an interspecies electron carrier in a syntrophic acetate-oxidizing anaerobic microorganism in coculture with methanogens. J. Biosci. Bioeng. 91, 294–298. https://doi.org/10.1016/S1389-1723(01)80137-7.

Heijnen, J.J., Kleerebezem, R., 2010. Bioenergetics of Microbial Growth. Encycl. Ind. Biotechnol. Bioprocess Biosep. Cell Technol. 1–66. https://doi.org/10.1002/9780470054581.eib084.

Heijnen, J.J., Van Dijken, J.P., 1992. In search of a thermodynamic description of biomass yields for the chemotrophic growth of microorganisms. Biotechnol. Bioeng. 39, 833–858. https://doi.org/10.1002/bit.260390806.

Heukelekian, H., 1958. Basic principles of sludge digestion. Biol. Treat. Sew. Ind. Wastes 2, 25.

Hoh, C.Y., Cord-Ruwisch, R., 1996. A practical kinetic model that considers endproduct inhibition in anaerobic digestion processes by including the equilibrium constant. Biotechnol. Bioeng. 51, 597–604. https://doi.org/10.1002/(SICI)1097-0290(19960905)51:5*597::AID-BIT12*3.0.CO;2-F.

Jin, Q., Bethke, C.M., 2007. The thermodynamics and kinetics of microbial metabolism. Am. J. Sci. 307, 643–677. https://doi.org/10.2475/04.2007.01.

IWA Task Group for, 2005. Mathematical Modelling of Anaerobic Digestion Processes. https://doi.org/10.2166/9781780403052.

Jin, Q., Bethke, C.M., 2003. A New Rate Law describing Microbial Respiration. Appl. Environ. Microbiol. 69, 2340–2348. https://doi.org/10.1128/AEM.69.4.2340-2348.2003.

Kleerebezem, R., Stams, A.J., 2000. Kinetics of syntrophic cultures: a theoretical treatise on butyrate fermentation. Biotechnol. Bioeng. 67, 529–543. https://doi.org/10.1002/(sici)1097-0290(20000305)67:5*529::aid-bit4*3.0.co;2-q.

Kleerebezem, R., Van Loosdrecht, M.C.M., 2010. A Generalized Method for Thermodynamic State Analysis of Environmental Systems. Crit. Rev. Environ. Sci. Technol. 40, 1–54. https://doi.org/10.1080/10643380802000974.

Leurent, A., Moscoviz, R., 2022. Modeling a propionate-oxidizing syntrophic coculture using thermodynamic principles. Biotechnol. Bioeng. 119, 2423–2436. https://doi.org/10.1002/bit.28156.

McCarty, P.L., Smith, D.P., 2002. Anaerobic wastewater treatment [WWW Document]. ACS Publ. https://doi.org/10.1021/es00154a002.

McInerney, M.J., Bryant, M.P., 1981. Basic Principles of Bioconversions in Anaerobic Digestion and Methanogenesis, in: Sofer, S.S., Zaborsky, O.R. (Eds.), Biomass Conversion Processes for Energy and Fuels. Springer US, Boston, MA, pp. 277–296. https://doi.org/10.1007/978-1-4757-0301-6_15.

Meegoda, J.N., Li, B., Patel, K., Wang, L.B., 2018. A Review of the Processes, Parameters, and Optimization of Anaerobic Digestion. Int. J. Environ. Res. Public Health 15, 2224. https://doi.org/10.3390/ijerph15102224.

Mo, R., Guo, W., Batstone, D., Makinia, J., Li, Y., 2023. Modifications to the anaerobic digestion model no. 1 (ADM1) for enhanced understanding and application of the anaerobic treatment processes – A comprehensive review. Water Res. 244, 120504. https://doi.org/10.1016/j.watres.2023.120504.

Montag, D., Schink, B., 2018. Formate and Hydrogen as Electron Shuttles in Terminal Fermentations in an Oligotrophic Freshwater Lake Sediment. Appl. Environ. Microbiol. 84, e01572–e1618. https://doi.org/10.1128/AEM.01572-18.

Montecchio, D., Esposito, G., Gagliano, M.C., Gallipoli, A., Gianico, A., Braguglia, C.M., 2017. Syntrophic acetate oxidation during the two-phase anaerobic digestion of waste activated sludge: Microbial population, Gibbs free energy and kinetic modelling. Int. Biodeterior. Biodegrad. 125, 177–188. https://doi.org/10.1016/j.ibiod.2017.09.017.

Pan, X., Angelidaki, I., Alvarado-Morales, M., Liu, H., Liu, Y., Huang, X., Zhu, G., 2016. Methane production from formate, acetate and H2/CO2; focusing on kinetics and microbial characterization. Bioresour. Technol. 218, 796–806. https://doi.org/10.1016/j.biortech.2016.07.032.

Pantaleo, A., Gennaro, B.D., Shah, N., 2013. Assessment of optimal size of anaerobic co-digestion plants: an application to cattle farms in the province of Bari (Italy). Renew. Sustain. Energy Rev. 20, 57–70. https://doi.org/10.1016/j.rser.2012.11.068.

Patón, M., Rodríguez, J., 2019a. Integration of bioenergetics in the ADM1 and its impact on model predictions. Water Sci. Technol. 80, 339–346. https://doi.org/10.2166/wst.2019.279.

Pedregosa, F., Varoquaux, G., Gramfort, A., Michel, V., Thirion, B., Grisel, O., Blondel, M., Prettenhofer, P., Weiss, R., Dubourg, V., Vanderplas, J., Passos, A., Cournapeau, D., Brucher, M., Perrot, M., Duchesnay, É., 2011. Scikit-learn: Machine Learning in Python. J. Mach. Learn. Res. 12, 2825–2830.

Patón, M., Rodríguez, J., 2019b. A compilation and bioenergetic evaluation of syntrophic microbial growth yields in anaerobic digestion. Water Res. 159, 176–183. https://doi.org/10.1016/j.watres.2019.05.013.

Rajagopal, R., Massé, D.I., Singh, G., 2013. A critical review on inhibition of anaerobic digestion process by excess ammonia. Bioresour. Technol. 143, 632–641. https://doi.org/10.1016/j.biortech.2013.06.030.

Raposo, F., Borja, R., Martín, M.A., Martín, A., de la Rubia, M.A., Rincón, B., 2009. Influence of inoculum–substrate ratio on the anaerobic digestion of sunflower oil cake in batch mode: Process stability and kinetic evaluation. Chem. Eng. J. 149, 70–77. https://doi.org/10.1016/j.cej.2008.10.001.

Rieger, L., Gillot, S., Langergraber, G., Ohtsuki, T., Shaw, A., Takács, I., Winkler, S., 2012. Guidelines for Using Activated Sludge Models. IWA Publishing. https://doi.org/10.2166/9781780401164.

Rivera-Salvador, V., López-Cruz, I.L., Espinosa-Solares, T., Aranda-Barradas, J.S., Huber, D.H., Sharma, D., Toledo, J.U., 2014. Application of Anaerobic Digestion Model No. 1 to describe the syntrophic acetate oxidation of poultry litter in thermophilic anaerobic digestion. Bioresour. Technol. 167, 495–502. https://doi.org/10.1016/j.biortech.2014.06.008.

Schink, B., 1997. Energetics of syntrophic cooperation in methanogenic degradation. Microbiol Mol Biol Rev 61, 262–280. https://doi.org/10.1128/mmbr.61.2.262-280.1997.

Schnürer, A., Nordberg, Å., 2008. Ammonia, a selective agent for methane production by syntrophic acetate oxidation at mesophilic temperature. Water Sci. Technol. 57, 735–740. https://doi.org/10.2166/wst.2008.097.

Scholten, J.C.M., Conrad, R., 2000. Energetics of Syntrophic Propionate Oxidation in Defined batch and Chemostat Cocultures. Appl. Environ. Microbiol. 66, 2934–2942. https://doi.org/10.1128/AEM.66.7.2934-2942.2000.

Singh, A., Schnürer, A., Dolfing, J., Westerholm, M., 2023. Syntrophic entanglements for propionate and acetate oxidation under thermophilic and high-ammonia conditions. ISME J. 17, 1966–1978. https://doi.org/10.1038/s41396-023-01504-y.

Uhlenhut, F., Schlüter, K., Gallert, C., 2018. Wet biowaste digestion: ADM1 model improvement by implementation of known genera and activity of propionate oxidizing bacteria. Water Res. 129, 384–393. https://doi.org/10.1016/j.watres.2017.11.012.

Viancelli, A., Michelon, W., ElMahdy, E.M., 2019. Current Efforts for the Production and Use of Biogas Around the World, in: Treichel, H., Fongaro, G. (Eds.), Improving Biogas Production: Technological Challenges, Alternative Sources, Future Developments. Springer International Publishing, Cham, pp. 277–287. https://doi.org/10.1007/978-3-030-10516-7_13.

Virtanen, P., Gommers, R., Oliphant, T.E., Haberland, M., Reddy, T., Cournapeau, D., Burovski, E., Peterson, P., Weckesser, W., Bright, J., van der Walt, S.J., Brett, M., Wilson, J., Millman, K.J., Mayorov, N., Nelson, A.R.J., Jones, E., Kern, R., Larson, E., Carey, C.J., Polat, İ., Feng, Y., Moore, E.W., VanderPlas, J., Laxalde, D., Perktold, J., Cimrman, R., Henriksen, I., Quintero, E.A., Harris, C.R., Archibald, A.M., Ribeiro, A.H., Pedregosa, F., van Mulbregt, P., 2020. SciPy 1.0: fundamental algorithms for scientific computing in Python. Nat. Methods 17, 261–272. https://doi.org/10.1038/s41592-019-0686-2.

Wallrabenstein, C., Hauschild, E., Schink, B., 1994. Pure culture and cytological properties of 'Syntriphobacter wolini'. FEMS Microbiol. Lett. 123, 249–254. https://doi.org/10.1111/j.1574-6968.1994.tb07232.x.

Wang, H., Lehtomäki, A., Tolvanen, K., Puhakka, J., Rintala, J., 2009. Impact of crop species on bacterial community structure during anaerobic co-digestion of crops and cow manure. Bioresour. Technol. 100, 2311–2315. https://doi.org/10.1016/j.biortech.2008.10.040.

Weng, N., Najafabadi, H.N., Westerholm, M., 2025. Disruption-induced changes in syntrophic propionate and acetate oxidation: flocculation, cell proximity, and microbial activity. Biotechnol. Biofuels Bioprod. 18, 45. https://doi.org/10.1186/s13068-025-02644-3.

Weng, N., Singh, A., Ohlsson, J.A., Dolfing, J., Westerholm, M., 2024. Catabolism and interactions of syntrophic propionate- and acetate oxidizing microorganisms under mesophilic, high-ammonia conditions. Front. Microbiol. 15, 1389257. https://doi.org/10.3389/fmicb.2024.1389257.

Westerholm, M., Dolfing, J., Schnürer, A., 2019. Growth Characteristics and Thermodynamics of Syntrophic Acetate Oxidizers. Environ. Sci. Technol. 53, 5512–5520. https://doi.org/10.1021/acs.est.9b00288.

Westerholm, M., Dolfing, J., Sherry, A., Gray, N.D., Head, I.M., Schnürer, A., 2011. Quantification of syntrophic acetate-oxidizing microbial communities in biogas processes. Environ. Microbiol. Rep. 3, 500–505. https://doi.org/10.1111/j.1758-2229.2011.00249.x.

Westerholm, M., Liu, T., Schnürer, A., 2020. Comparative study of industrial-scale high-solid biogas production from food waste: Process operation and microbiology. Bioresour. Technol. 304. https://doi.org/10.1016/j.biortech.2020.122981.

Wett, B., Takács, I., Batstone, D., Wilson, C., Murthy, S., 2014. Anaerobic model for high-solids or high-temperature digestion – additional pathway of acetate oxidation. Water Sci. Technol. 69, 1634–1640. https://doi.org/10.2166/wst.2014.047.

Yang, Z., Sun, H., Zhao, Q., Kurbonova, M., Zhang, R., Liu, G., Wang, W., 2020. Long-term evaluation of bioaugmentation to alleviate ammonia inhibition during anaerobic digestion: Process monitoring, microbial community response, and methanogenic pathway modeling. Chem. Eng. J. 399. https://doi.org/10.1016/j.cej.2020.125765.

Zhao, X., Li, L., Wu, D., Xiao, T., Ma, Y., Peng, X., 2019. Modified Anaerobic Digestion Model No. 1 for modeling methane production from food waste in batch and semi-continuous anaerobic digestions. Bioresour. Technol. 271, 109–117. https://doi.org/10.1016/j.biortech.2018.09.091.